

# A miniature reflective micro-force sensor based on a microfiber coupler

Ye Chen,<sup>1</sup> Shao-cheng Yan,<sup>1</sup> Xin Zheng,<sup>1</sup> Fei Xu,<sup>1,\*</sup> and Yan-qing Lu<sup>1,2</sup>

<sup>1</sup>National Laboratory of Solid State Microstructures and College of Engineering and Applied Sciences, Nanjing University, Nanjing 210093, China

<sup>2</sup>yqlu@nju.edu.cn

<sup>3</sup>feixu@nju.edu.cn

**Abstract:** A compact highly sensitive microfiber coupler based reflective micro-force sensor is presented. The device is fabricated by fusing two twisted optical fibers and then connecting two of the pigtails to form a Sagnac loop. The sensor has a high force sensitivity of  $\sim 3754$  nm/N which is three orders of magnitude larger than traditional optical fiber force sensors, and a low detection limit of  $\sim 1.6$   $\mu$ N. The good repeatability is also shown in this paper.

©2014 Optical Society of America

**OCIS codes:** (230.1150) All-optical devices; (060.2340) Fiber optics components; (060.1810) Buffers, couplers, routers, switches, and multiplexers; (060.2370) Fiber optics sensors.

---

## References and links

1. S. Huang, F. Luo, and Y. Pan, "A fiber optic sensor for measuring distributed forces," *J. Intell. Mater. Syst. Struct.* **5**(3), 427–431 (1994).
2. K. S. Lau, T. L. Chan, and K. H. Wong, "Force measurement by visibility modulated fiber optic sensor," *Appl. Opt.* **38**(34), 7163–7164 (1999).
3. W. Zhang, X. Dong, Q. Zhao, G. Kai, and S. Yuan, "FBG-type sensor for simultaneous measurement of force (or displacement) and temperature based on bilateral cantilever beam," *IEEE Photonics Technol. Lett.* **13**(12), 1340–1342 (2001).
4. L. Xue, Q. Zhao, J. Liu, G. Huang, T. Guo, and X. Dong, "Force sensing with temperature self-compensated based on a loop thin-wall section beam," *IEEE Photonics Technol. Lett.* **18**(1), 271–273 (2006).
5. B. Dong, Q. Zhao, L. Zhao, L. Jin, Y. Miao, T. Liao, and X. Zeng, "Simultaneous measurement of temperature and force based on a special-strain-function-chirped FBG," *Sens. Actuators A Phys.* **147**(1), 169–172 (2008).
6. J. Hao, Z. Cai, J. H. Ng, Y. Gong, and P. Varghese, "Simultaneous temperature and lateral force measurement using simple arc-shaped FBG sensor module," *Electron. Lett.* **42**(25), 1446–1447 (2006).
7. L. M. Tong, R. R. Gattass, J. B. Ashcom, S. L. He, J. Y. Lou, M. Y. Shen, I. Maxwell, and E. Mazur, "Subwavelength-diameter silica wires for low-loss optical wave guiding," *Nature* **426**(6968), 816–819 (2003).
8. M. Sumetsky, Y. Dulashko, J. M. Fini, A. Hale, and D. J. DiGiovanni, "The microfiber loop resonator: theory, experiment, and application," *J. Lightwave Technol.* **24**(1), 242–250 (2006).
9. X. S. Jiang, L. M. Tong, G. Vienne, X. Guo, A. Tsao, Q. Yang, and D. R. Yang, "Demonstration of optical microfiber knot resonator," *Appl. Phys. Lett.* **88**(22), 223501 (2006).
10. F. Xu and G. Brambilla, "Manufacture of 3-D microfiber coil resonators," *IEEE Photonics Technol. Lett.* **19**(19), 1481–1483 (2007).
11. W. Luo, J. L. Kou, Y. Chen, F. Xu, and Y. Q. Lu, "Ultra-highly sensitive surface-corrugated microfiber Bragg grating force sensor," *Appl. Phys. Lett.* **101**(13), 133502 (2012).
12. Y. Jung, G. Brambilla, and D. J. Richardson, "Optical microfiber coupler for broadband single-mode operation," *Opt. Express* **17**(7), 5273–5278 (2009).
13. Y. Jung, R. Chen, R. Ismaeel, G. Brambilla, S.-U. Alam, I. P. Giles, and D. J. Richardson, "Dual mode fused optical fiber couplers suitable for mode division multiplexed transmission," *Opt. Express* **21**(20), 24326–24331 (2013).
14. P. Wang, M. Ding, G. Brambilla, Y. Semenova, Q. Wu, and G. Farrell, "Resolution improvement of a ratiometric wavelength measurement system by using an optical microfiber coupler," in *2012 Symposium on Photonics and Optoelectronics (SOPO)*, (Shanghai, 2012), pp. 1–4.
15. M. Ding, P. Wang, and G. Brambilla, "A microfiber coupler tip thermometer," *Opt. Express* **20**(5), 5402–5408 (2012).
16. M. Ding, P. Wang, J. Wang, and G. Brambilla, "FIB-milled gold-coated singlemode-multimode-singlemode fiber tip refractometer," *IEEE Photonics Technol. Lett.* **26**(3), 239–241 (2014).
17. F. P. Payne, C. D. Hussey, and M. S. Yataki, "Polarisation analysis of strongly fused and weakly fused tapered couplers," *Electron. Lett.* **21**(13), 561–563 (1985).
18. C. R. Liao, D. N. Wang, and Y. Wang, "Microfiber in-line Mach-Zehnder interferometer for strain sensing," *Opt. Lett.* **38**(5), 757–759 (2013).

19. O. Frazão, S. F. O. Silva, A. Guerreiro, J. L. Santos, L. A. Ferreira, and F. M. Araújo, "Strain sensitivity control of fiber Bragg grating structures with fused tapers," *Appl. Opt.* **46**(36), 8578–8582 (2007).
  20. G. Brambilla, V. Finazzi, and D. J. Richardson, "Ultra-low-loss optical fiber nanotapers," *Opt. Express* **12**(10), 2258–2263 (2004).
  21. M. S. Yataki, D. N. Payne, and M. P. Varnham, "All-fibre polarising beamsplitter," *Electron. Lett.* **21**(6), 249–251 (1985).
  22. J. D. Love and M. Hall, "Polarisation modulation in long couplers," *Electron. Lett.* **21**, 519–521 (1985).
- 

## 1. Introduction

Force sensing is of great importance in many applications such as structure inspection of aircraft, civil infrastructure and earthquake monitoring. Recently fiber based force sensors have been developed rapidly because of their insensitivity to electromagnetic fields, light weight, minimal intrusiveness, ease of termination and coupling. Different types of force sensors based on highly birefringent (Hi-Bi) fibers, Mach-Zehnder (M-Z) interferometers, fiber Bragg gratings (FBGs), etc. have been demonstrated. The Hi-Bi fiber force sensor [1] needs to use expensive fiber. The M-Z interferometer-based force sensor [2] has a complicated sensing structure and is hard to be fabricated. Force sensor using FBG [3–6] mainly operates by monitoring the shift of Bragg wavelength which is caused by applied force. In order to realize the temperature and force discrimination, the FBG based sensor usually has a complicated structure. In addition, FBG is very fragile and the sensitivity of a typical FBG based force sensor is only  $\sim 1$  nm/N. However, in many practical applications, particularly micro-force measurements, the force sensor should be low-cost, compact, simply structured, easily fabricated as well as highly sensitive and have a low detection limit.

Since a seminal paper published in 2003 [7], microfiber has received a lot of attention because of its low loss, large evanescent field, strong confinement, configurability and robustness. Compact devices based on microfiber such as loop resonators [8], knot resonators [9], and coil resonators [10] have been investigated. Recently, a microfiber FBG based force sensor was demonstrated by Luo *et al.* [11] with a sensitivity of  $\sim 3146$  nm/N. But the fabrication method using focused ion beam (FIB) leads to a high cost and low production. Moreover, the fragile structure and high loss ( $\sim 13$  dB) limit its application. In 2009, a broadband single mode microfiber coupler (MFC) was demonstrated by Jung *et al.* [12]. MFCs have many applications in optical communication [13], wavelength measurement [14] and sensing [15] due to their good performance and low cost. In reference [15], Ding *et al.* demonstrated a compact thermometer based on a MFC tip for high temperature sensing. The device had a large loss ( $\sim 20$  dB) mainly because of the poor reflection at the tip end face. Further processing is needed to enhance the reflection of MFC tip [16]. In this paper, a low loss miniature highly sensitive force sensor based on a MFC is presented. We constructed a Sagnac loop to reflect the light and gained a low loss of  $\sim 1$  dB which was mainly due to the insertion loss caused by the bare fiber adaptors. The fabricated device has the advantages of low cost (made by commercial single-mode fibers), simple structure (fused optical fiber coupler), compact size (microfiber based device), easily fabricating (flame-brushing method) as well as high sensitivity ( $\sim 3754$  nm/N) and low detection limit ( $< 1.6$   $\mu$ N).

## 2. Theoretical analysis

Figure 1 shows the schematic of a MFC. MFCs are manufactured by laterally fusing and tapering two twisted optical fibers. A MFC comprises two conical transition regions, a central uniform waist region and four input/output ports: light injected into ports  $P_1$  or  $P_2$  exits from ports  $P_3$  and  $P_4$ .

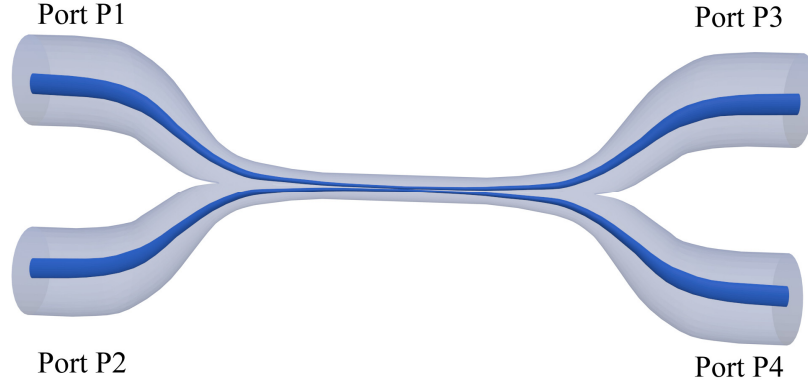


Fig. 1. Schematic of a MFC.

The MFC can be assumed as a weakly fused coupler, approximated by two touching cylindrical waveguides. The coupling coefficients for the  $x$  and  $y$  polarizations are given by [17]:

$$C_x = \frac{2^{3/2} (n_1^2 - n_0^2)^{1/2} U_\infty^2 (2n_1^2 V + 1)}{n_1^3 a (\sqrt{\pi}) V^{7/2}} \quad (1)$$

$$C_y = \frac{2^{3/2} (n_1^2 - n_0^2)^{1/2} U_\infty^2 (2n_1^2 V - 1)}{n_1^3 a (\sqrt{\pi}) V^{7/2}} \quad (2)$$

where  $n_1$  and  $n_0$  refer to the refractive indices of silica and air,  $a$  denotes the diameter of one of the microfibers,  $U_\infty = 2.405$  and  $V = [(2\pi a)/\lambda](n_1^2 - n_0^2)^{1/2}$ .

Figure 2 demonstrates the structure of our device. We connect ports  $P_3$  and  $P_4$  together to form a Sagnac loop. If light entering the input port  $P_1$  is unpolarized, the normalized power at the output port  $P_2$  can be described by:

$$P_2 = \frac{1}{2} \{ 1 + \cos[2(\overline{C}_x + \overline{C}_y)L_{\text{coupler}}] \cos[2(\overline{C}_x - \overline{C}_y)L_{\text{coupler}}] \} \quad (3)$$

where  $L_{\text{coupler}}$  is the coupling length of the MFC,  $\overline{C}_x$  and  $\overline{C}_y$  are the values of Eqs. (1) and (2) averaged over the whole coupling region. Because of the large modal size and the relatively small overlap, the contribution of the transition regions is negligible.

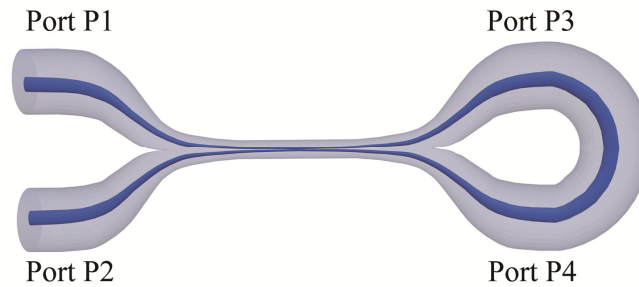


Fig. 2. Structure of the miniature MFC Sagnac loop.

Equations (1)–(3) exhibit that the output power depends on the wavelength  $\lambda$ , refractive index  $n_1$ , coupling length  $L_{\text{coupler}}$ , and coupler radial size  $2a$ . A longitudinal mechanical force  $f$

applied to the device will induce both refractive index  $n_1$  and coupling length  $L_{\text{coupler}}$  to change, which can be predicted by following formulas [11, 18, 19]:

$$\frac{\Delta L_{\text{coupler}}}{L_{\text{coupler}}} = \varepsilon_{\text{coupler}} = \frac{f}{EA_{\text{coupler}}} \quad (4)$$

$$\frac{\Delta n_1}{n_1} = -\frac{f}{EA_{\text{coupler}}} \times P \quad (5)$$

$$P = \frac{n_1^2}{2} [p_{12} - \nu(p_{11} + p_{12})] \quad (6)$$

where  $E$  is the Young's modulus of the fiber material,  $\varepsilon_{\text{coupler}}$  is the applied strain on coupling region, and  $A_{\text{coupler}}$  is the area of coupling region cross section which can be calculated by  $A_{\text{coupler}} = 2\pi(a/2)^2$ ,  $\nu$  is the Poisson ratio,  $p_{11}$  and  $p_{12}$  are the components of Pockel's strain-optical tensor of the fiber material, respectively.  $P$  is the effective photo-elastic coefficient.

The force dependence of the device output spectrum around 1550 nm can be evaluated by assuming first  $1 \times 10^{-4}$  N and then  $2 \times 10^{-4}$  N longitudinal mechanical forces are applied on the device, respectively. We assume  $L_{\text{coupler}} = 1$  cm,  $a = 1.6$   $\mu\text{m}$ ,  $p_{11} = 0.113$ ,  $p_{12} = 0.252$ ,  $\nu = 0.17$ , and  $E = 73$  GPa in our calculation, respectively. The refractive index  $n_1$  and coupling length  $L_{\text{coupler}}$  will then vary with the force and result in the change of the output spectrum. Figure 3 shows the output power variation under three different mechanical forces. The peak wavelength has a blueshift of  $\sim 734$  pm when the force increases from 0 N to  $2 \times 10^{-4}$  N, with an average sensitivity of  $\sim 3670$  nm/N.

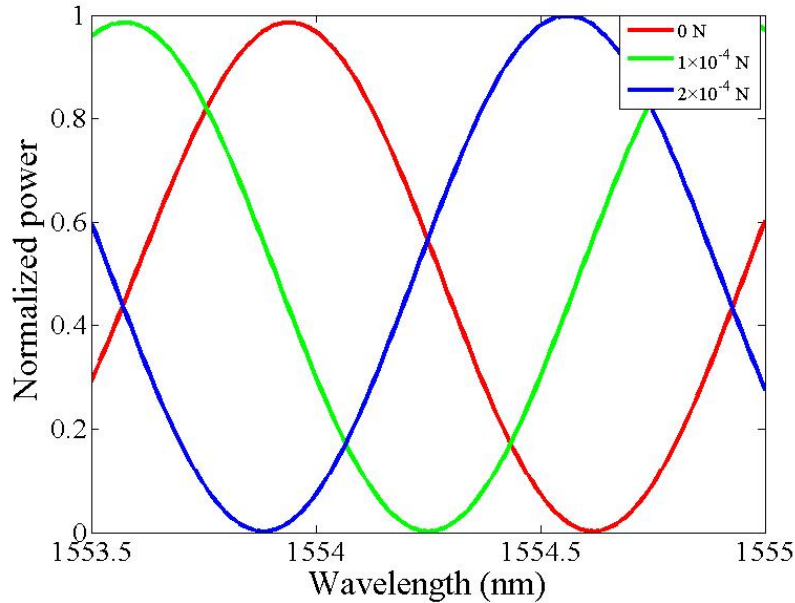


Fig. 3. The calculated output power from port  $P_2$  under three different mechanical forces.

We then calculate the dependence of force sensitivity  $S$  on the microfiber diameter  $a$  around 1550 nm wavelength. As revealed in Fig. 4,  $S$  increases quickly with the decreasing diameter.

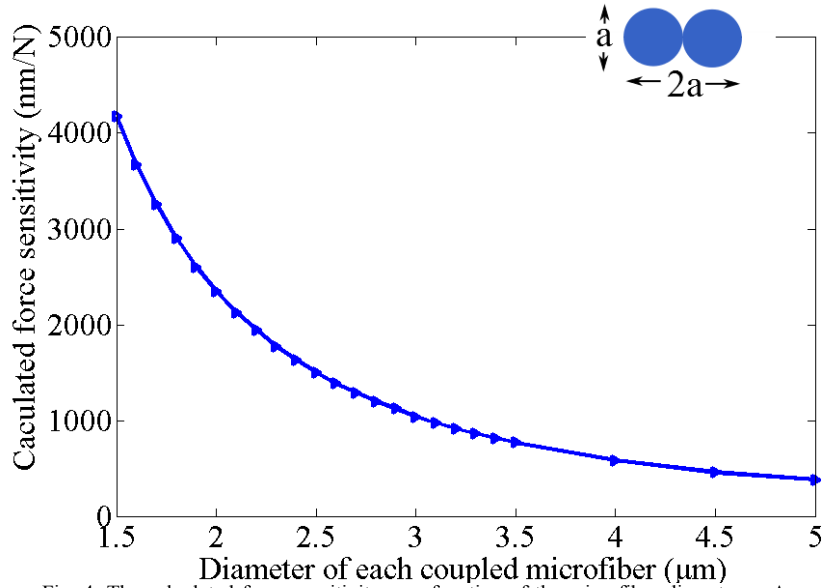


Fig. 4. The calculated force sensitivity as a function of the microfiber diameter  $a$ . A smaller diameter will cause a higher sensitivity. Inset: cross section of the MFC coupling region in the “weakly fusing” approximation.

### 3. Experiment and discussion

First, a MFC was fabricated from two standard telecom optical fibers (SMF-28, Corning, NY, USA) using the flame brushing method [20]. Figures 5(a) and 5(b) illustrate the microscope images of the MFC: the diameter of each coupled microfiber was  $\sim 1.6 \mu\text{m}$ , the coupling region length was  $\sim 1 \text{ cm}$ . Then, ports  $P_3$  and  $P_4$  were connected together using a commercial fusion splicer to form a Sagnac interferometer.

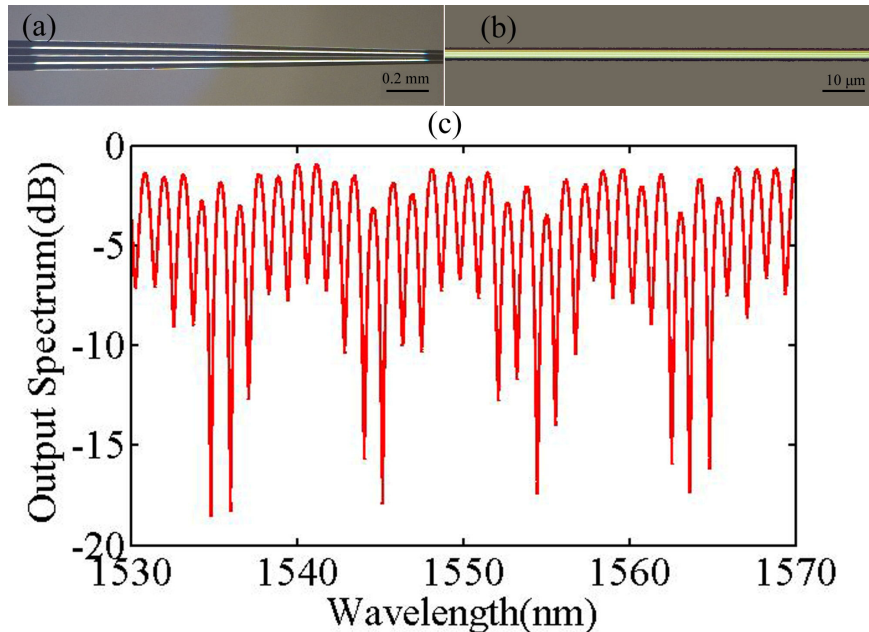


Fig. 5. Microscope images of (a) the transition region and (b) coupling region of the MFC, the diameter of each coupled microfiber is  $\sim 1.6 \mu\text{m}$ ; (c) Output spectrum at port  $P_2$ .

The spectral characterization of our device was carried out by connecting a supercontinuum (SC) source (NKT Photonics), with emission over the wavelength range 1200-1700 nm, to port P<sub>1</sub> and an optical spectrum analyzer (OSA) (AQ6317C, Yokogawa, Japan) to port P<sub>2</sub>. The output spectrum at room temperature is presented in Fig. 5(c). It shows a multi-peak pattern due to lower-order symmetric and anti-symmetric supermodes interference in the coupling region. We can see a slow modulation of the spectral envelope which can be explained by the different coupling coefficients for *x* and *y* polarizations [21, 22].

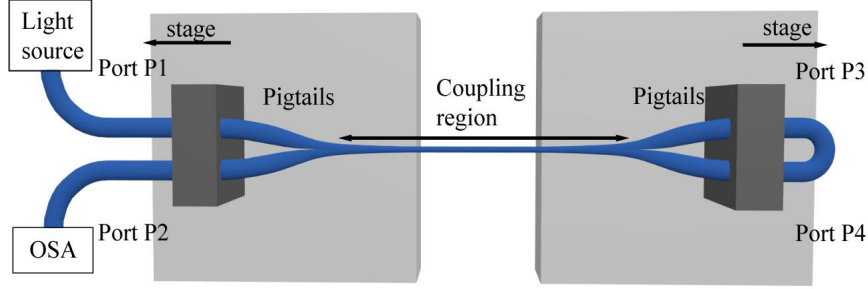


Fig. 6. Schematic of the measurement setup.

The measurement setup is shown in Fig. 6. The device was held on two stretch stages. Port P<sub>1</sub> was connected to the broadband light source (NKT, SuperK Versa) and port P<sub>2</sub> was connected to the OSA (Ando AQ6317C). Light from the source goes through the sample and then into the OSA. As we controlled the stages to move away from each other, a longitudinal force would be applied on the coupler and thus influence the refractive index and coupling length. As the force changed the lengths of both the coupling region and pigtailed:

$$L_{\text{coupler}} + L_{\text{pigtail}} = L_{\text{fiber}} \quad (7)$$

$$\Delta L_{\text{coupler}} + \Delta L_{\text{pigtail}} = L_{\text{stretch}} \quad (8)$$

where  $L_{\text{coupler}}$  and  $L_{\text{pigtail}}$  refer to the length of coupler region and fiber pigtailed between the two stretch stages.  $L_{\text{fiber}}$  is the total length of the above two parts, i.e. the distance between the two stretch stages. In our experiment  $L_{\text{fiber}} = 1.3$  cm.  $\Delta L_{\text{coupler}}$  and  $\Delta L_{\text{pigtail}}$  are the length changes of the coupling and pigtail regions, respectively. The forces applied to the coupling region and to the pigtail region are equal [18]:

$$\varepsilon_{\text{coupler}} EA_{\text{coupler}} = \varepsilon_{\text{pigtail}} EA_{\text{pigtail}} \quad (9)$$

where  $A_{\text{coupler}}$  and  $A_{\text{pigtail}}$  are the cross sectional areas of coupling and pigtail regions, respectively.  $\varepsilon_{\text{coupler}}$  and  $\varepsilon_{\text{pigtail}}$  refer to the applied strain on the relevant region. Then the relationship between the stretched distance and the force can be predicted by using Eqs. (4) and (7)–(9). In our experiment, each stage moved 1  $\mu\text{m}$  per-step,  $L_{\text{stretch}} = 2$   $\mu\text{m}$ , thus the applied force  $f$  increased  $5.86 \times 10^{-5}$  N per-step.

Figure 7 reports the output spectrum of the device under different forces. When the applied force rises from  $4.10 \times 10^{-4}$  N to  $5.27 \times 10^{-4}$  N, the peak wavelength blueshifts from 1552.96 nm to 1552.53 nm.

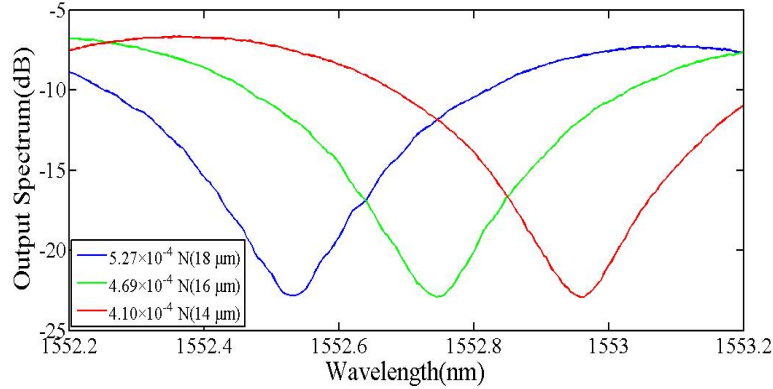


Fig. 7. Output spectrum of the device around the peak wavelength 1553 nm under different forces.

The sensitivity is defined as the wavelength shift associated to the force change. Figure 8 illustrates the peak wavelength shift against the applied force. In this experiment, the applied force varied from 0 N to  $7.03 \times 10^{-4}$  N (i.e. the stretched length rose from 0  $\mu\text{m}$  to 24  $\mu\text{m}$ ).

The force sensitivity  $S$  is  $\sim 3754$  nm/N, which is three orders of magnitude larger than that of traditional optical fiber force sensors. The explanation for the difference between the theoretical calculation and experimental data could be the imperfect weakly fused coupler simplification in theory and the refractive index error. The sensor detection limit can be defined as  $\delta\lambda_0/S$ , where  $\delta\lambda_0$  is the smallest measurable wavelength shift. Generally,  $\delta\lambda_0$  is limited by instrument resolution and is assumed as 1/50 of the full width at half maximum (FWHM) of the monitored resonance. The sensor detection limit was estimated to be  $\sim 1.6$   $\mu\text{N}$  for a FWHM of  $\sim 0.3$  nm. Lower detection limit ( $\sim \text{nN}$ ) possibly can be achieved with better instruments and optimized fabrication.

The force measurement repeatability was also evaluated by recording spectra with increasing and decreasing forces. As we can see from Fig. 8, data from the two curves coincide with each other, showing that the device has a good repeatability.

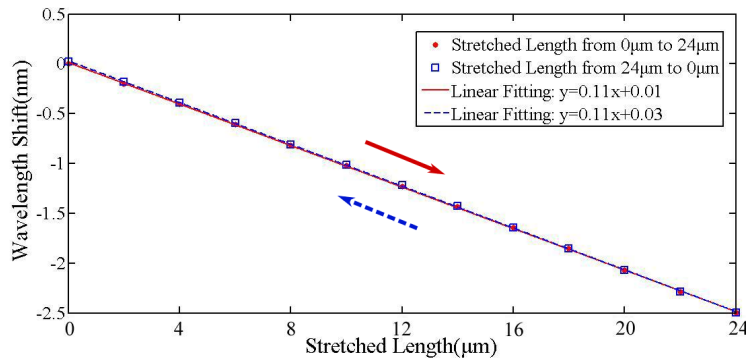


Fig. 8. Wavelength shift dependence on the stretched length. The red and blue curves refer to increasing and decreasing forces, respectively.

#### 4. Conclusion

In this paper, we demonstrate a compact highly-sensitive microfiber coupler based reflective micro-force sensor. The device is fabricated by fusing two twisted optical fibers (SMF-28) and then connecting two of the pigtails to form a Sagnac loop. The sensor has a high force sensitivity of  $\sim 3754$  nm/N with a good repeatability around the wavelength of 1553 nm, about three orders of magnitude larger than that of traditional optical fiber force sensors. The device

has a large potential in many applications such as micro-force detection, structure inspection of aircraft and earthquake monitoring.

### **Acknowledgments**

This work is supported by National 973 program under contract No. 2012CB921803 and 2011CBA00205, NSFC program No. 11074117 and National Science Fund for Excellent Young Scientists Fund (61322503) and National Science Fund for Distinguished Young Scholars (61225026). The authors also acknowledge the support from PAPD and the Fundamental Research Funds for the Central Universities. The authors thank Wei Guo, Bi-cai Zheng, and Guang-hao Shao for their kindly help.